The importance of the hook region of the cochlea for bone-conduction hearing

Namkeun Kim[†], Charles R. Steele[†], and Sunil Puria[†,‡],

[†]*Department of Mechanical Engineering, Stanford University, Stanford, California 94305, USA*

[‡]*Department of Otolaryngology-Head and Neck Surgery, Stanford University, Stanford, California 94305, USA*

SUPPORTING MATERIAL

In this Supporting Material section, the model responses (e.g., the middle-ear pressure-gain function, cochlear impedance, basilar-membrane velocity, and best-frequency map) are compared with published data in order to provide validation for the current finite-element (FE) model. In addition, cochlear responses to air-conducted (AC) and bone-conducted (BC) excitations were calculated, and also compared with those of the previous FE model.

Validation of the FE model

The model-validation procedures are similar to those used in a previous study with a box model (1), with similar results in terms of the middle-ear (ME) pressure-gain function, cochlear input impedance, basilar-membrane (BM) velocity at specific locations, and cochlear best-frequency (BF) map.

Middle-ear pressure-gain function

In Figure S1, the ME pressure-gain function from the FE model, expressed as the ratio of the scalae-fluid pressure near the oval window (OW) to the acoustic pressure in the ear canal at the tympanic membrane (TM), P_{OW}/P_{EC}, is shown and compared with results from the literature (2–5). The FE results were consistent with experimental data to within about 5 dB from 0.3 kHz to 10 kHz.

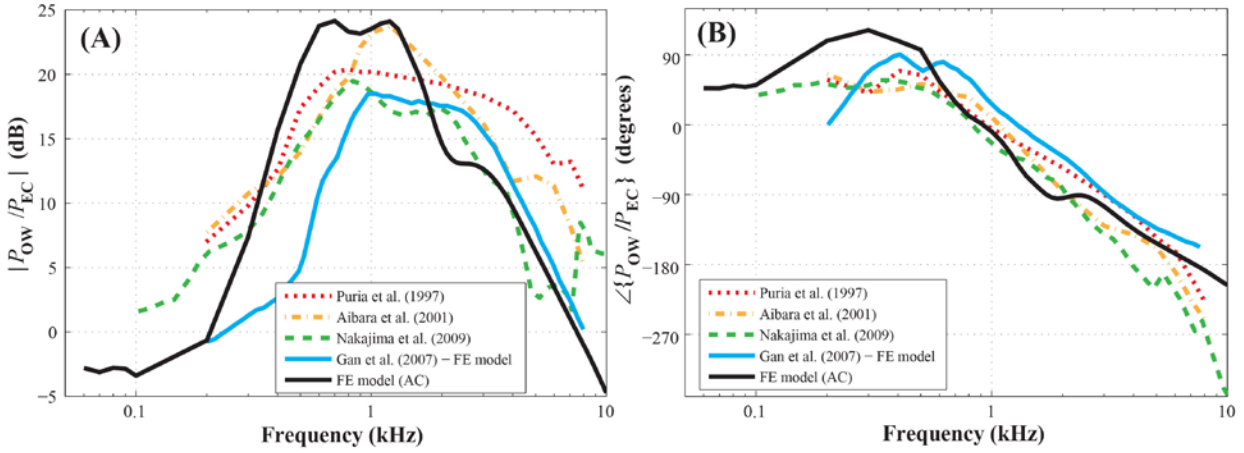

FIGURE S1. (A and B) The oval-window pressure, P_{OW}, to the ear-canal pressure, P_{EC}, middle-ear gain (P_{OW}/P_{EC}), for air-conducted (AC) excitation. (A) Magnitude in dB and (B) phase in degrees.

Cochlear input impedance

In Figure S2, the cochlear input impedance (Z_C) from the present model is shown alongside previous measured (3–6) and calculated (2) results. At frequencies below 0.5 kHz, the magnitude of Z_C for the current FE model falls within the range of the experimental data, but for higher frequencies it mostly remains somewhat above the comparison data in spite of their wide variance.

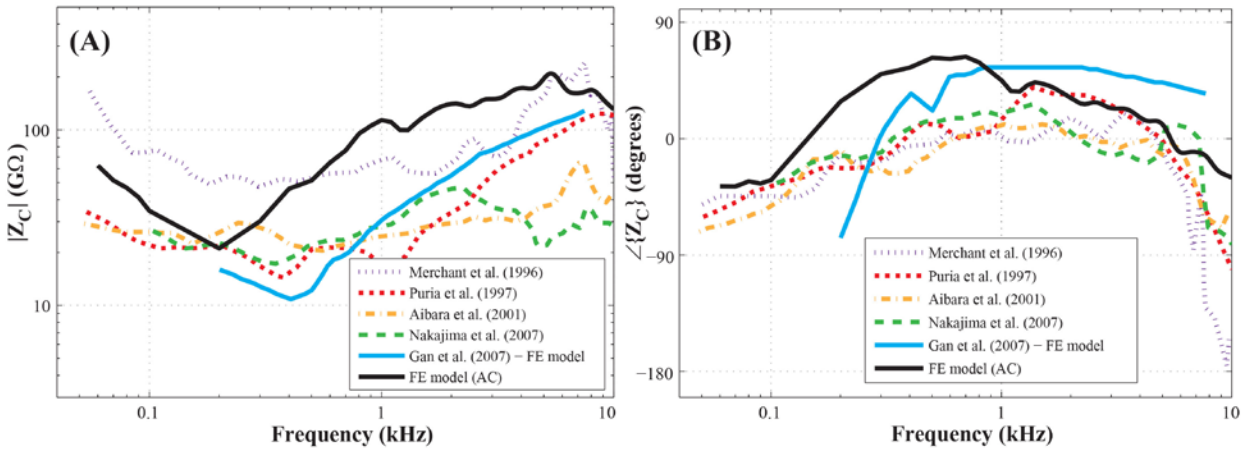

FIGURE S2. (A and B) Cochlear input impedance, Z_C, which is equal to P_{OW}/U_{OW}. (A) Magnitude in GΩ and (B) phase in degrees.

BM velocities at a specific location (χ = 12 mm)

The responses of V_{BM}, the velocity normal to the BM surface, to AC stimuli; and the relative BM velocity, ΔV_{BM}, to BC stimuli (where ΔV_{BM} is equal to V_{BM} minus the velocity of the bone, V_B), were measured at a specific BM location (approximately 12 *mm* from the base), and are shown in Figure S3. V_{BM} was normalized by the OW (i.e., stapes-footplate) velocity, V_{OW}, for AC stimuli. ΔV_{BM} was normalized by V_B for BC stimuli, and then $20\times log_{10}(\Delta V_{BM}/ V_B)$ was computed to represent '$\Delta V_{BM}/ V_B$' on a dB scale. For the model's AC results (Figure S3A), V_{BM}/V_{OW} reaches a maximum amplitude of 27 dB, between 4 and 5 kHz, which is reasonably consistent with the experimental data (7–8). For the model's BC results (Figure S3B), $\Delta V_{BM}/V_B$ reaches 21 dB for the maximum amplitude, at around 4 kHz, while the data from Stenfelt et al. (8) rises to 18 dB for the maximum amplitude, at around 2 kHz.

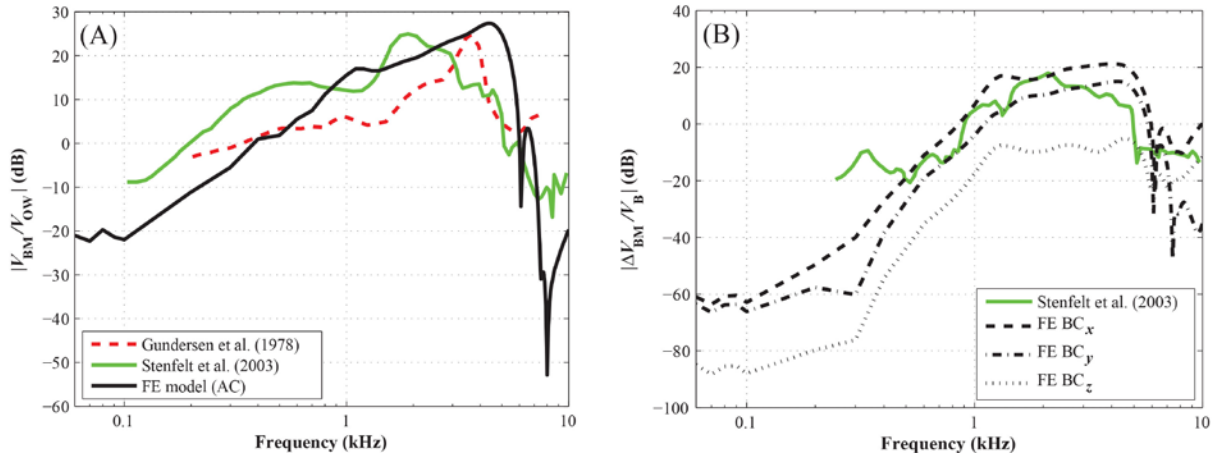

FIGURE S3. (A) The basilar-membrane (BM) velocity normalized by the stapes-footplate velocity, V_{BM}/V_{OW}, for AC excitation, and (B) the relative BM velocity ($\Delta V_{BM} = V_{BM} - V_B$) normalized by the BC bone-velocity input, $\Delta V_{BM}/V_B$, given for inputs in the direction of each of the three orthogonal axes, *x*, *y*, and *z* (*i.e.*, lateral, superior, and medial directions of the skull, respectively). The BM velocity for both modeled and experimental responses was calculated at χ = 12 *mm* from the RW.

Cochlear best-frequency map

The FE-simulated best-frequency (BF) cochlear map is shown in Figure S4, and is compared with the cochlear map estimated from an equation found in (9). The BF map from the FE model is in good agreement with the data except for the BFs below 200 Hz, which correspond to BM locations greater than χ = 30 *mm*. This agreement between the simulated and measured BF maps was achieved by iteratively tuning the elastic modulus values of the BM for AC excitation. It should be noted that the model's BF map is a serrated line rather than a smooth line like Greenwood's results for the following reason: in local regions where the curvature of the coiled BM is large, the width of the BM in the model does not increase smoothly along the length of the BM from base to apex, and as a result, the location of the node where the BM velocity is calculated ends up straying slightly from the centerline of the BM in these regions.

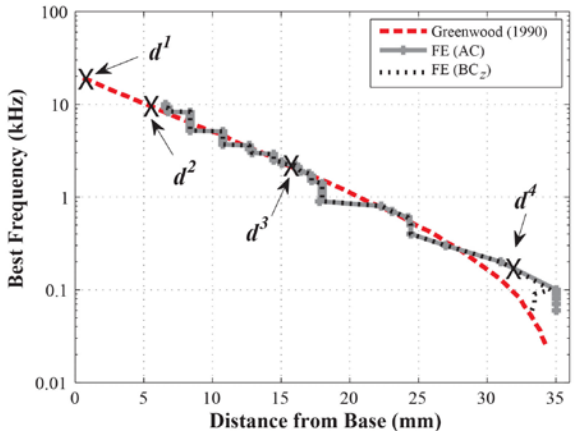

FIGURE S4. Simulated best-frequency (BF) maps for AC excitation and BC excitation given in the *z* direction, along with results from Greenwood (9). The results in the *x* and *y* directions were almost identical to the one shown for the *z*-directional excitation. 'X' marks on the BF plot indicate the four different BM locations (0.8, 5.8, 15.63, and 33.06 *mm*) for which the d^1, d^2, d^3, and d^4 directions are respectively defined.

Cochlear responses to AC and BC excitation

Having thus validated the FE model, the next step was to simulate and analyze the symmetric (fast-wave) and anti-symmetric (slow-wave) response characteristics of the scalae-fluid pressure and volume velocities of the OW and round window (RW) due to AC and BC excitations. Normalized BM-velocities are plotted along the length of the BM in Figures S5, S6, and S7, for particular input frequencies.

BM-velocity responses to AC and BC excitation

Figure S5 shows the simulated relative BM-velocity distribution along the length of the BM, $\Delta V_{\mathrm{BM}}(\chi)$, in response to BC excitations of the rigid bone forming the boundaries of the model. The results are shown for three frequencies: 0.5, 1, and 7 kHz. The BC cases are normalized with respect to the velocity magnitude of the rigid bone, V_{B}. Figure S5 also shows the BM-velocity distribution in response to AC excitation, $V_{\mathrm{BM}}(\chi)$, normalized by the corresponding stapes velocity, V_{OW}. The overall shape of the BM-velocity distribution magnitude for each respective frequency is similar among the different excitation cases, including between the AC- and BC-excitation cases. However, the primary difference among the three input-frequency cases (0.5, 1.0, and 7.0 kHz) is that their magnitudes are shifted with respect to one another. The phase responses for the different input frequencies are similarly shifted with respect to one another.

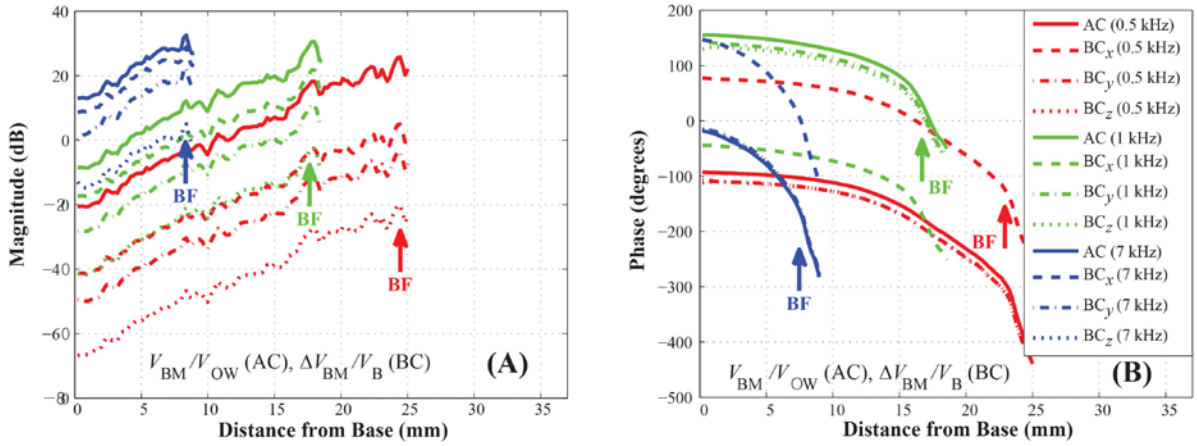

FIGURE S5. Magnitude (A) and Phase (B) of BM-velocity profiles along the length of the BM, $V_{BM}(\chi)$, normalized by the stapes velocity, V_{OW}, for AC excitation (solid lines); and the relative BM-velocity profile, $\Delta V_{BM}(\chi)$, normalized by the magnitude of the base bone velocity, V_B, for BC excitations. Excitation frequencies of 0.5, 1, and 7 kHz were used. The BC curves indicate the sensitivity of the cochlea to BC excitations in the *x* (dashed lines), *y* (dash-dotted lines), and *z* (dotted lines) directions. The legend applies to both (A) and (B), and the arrows labeled "BF" indicate the best-frequency locations on the BM corresponding to each stimulus frequency.

Normalization of the BM velocity by anti-symmetric and symmetric volume-velocity components

Figure S6 shows, for the present coiled-cochlea model, the BM-velocity (V_{BM}) and relative BM-velocity (ΔV_{BM}, where ΔV_{BM} is defined as '$V_{BM} - V_B$', with V_B being the BC velocity used to stimulate the model) distributions in response to AC and BC excitations, respectively. These quantities are normalized by both the anti-symmetric, U_A, and symmetric, U_S, volume-velocity components (in Figures S6A and S6B, respectively). The results are shown for 0.5, 1, and 7 kHz. As can be seen in Figure S6(A), the results for the different excitation cases show better alignment with each other when they are normalized by the anti-symmetric volume-velocity component, U_A (as compared to Figure S5A, in which the results are normalized by the stapes velocity and bone velocity for AC and BC, respectively). In the case of the 7 kHz results, the magnitudes of the normalized BM velocities (V_{BM}/U_A for AC and $\Delta V_{BM}/U_A$ for BC) show at most a 2–5 dB difference between one another, whereas for the other frequencies, 0.5 and 1 kHz, the corresponding normalized BM velocities for AC and BC stimuli overlap with one another such that they appear to form single lines. In contrast, when normalized by the symmetric volume-velocity component, U_S (Figure S6B), the results for a given frequency reveal misalignments between the different excitation methods. This demonstrates that the anti-symmetric volume-velocity component, U_A, correlates with the BM vibration better than the symmetric volume-velocity component, U_S. This was also the finding for the simplified box model (1).

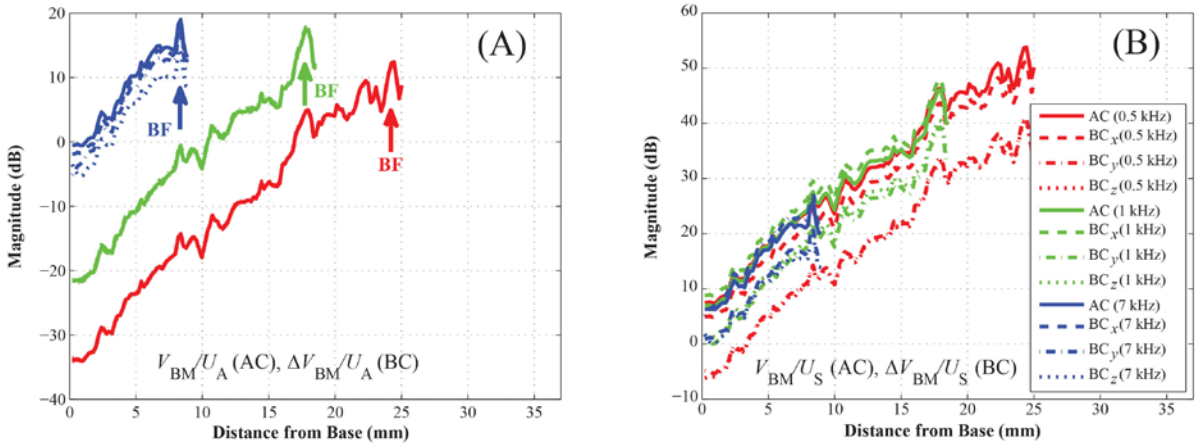

FIGURE S6. (A and B) BM velocity distributions along the length of the BM, $V_{BM}(\chi)$ and $\Delta V_{BM}(\chi)$ (defined as '$V_{BM} - V_B$', where V_B is the BC velocity used to stimulate the model), in response to AC and BC excitations, respectively, at 0.5, 1, and 7 kHz. The results are normalized by (A) the anti-symmetric volume-velocity (slow-wave) component, U_A, and (B) the symmetric volume-velocity (fast-wave) component, U_S.

Decomposition of the cochlear-fluid pressure into symmetric and anti-symmetric components

Figure S7 shows the anti-symmetric and symmetric pressure components, $P_A(\chi)$ and $P_S(\chi)$, normalized by U_A, at 1 and 7 kHz. In the figure, the magnitudes of $P_A(\chi)$ for different excitation cases become aligned with one another up to the corresponding BF position when normalized by U_A, whereas this is not the case for $P_S(\chi)/U_A$. This result follows a similar pattern to the normalized BM velocities ($V_{BM}(\chi)/U_A$ for AC and $\Delta V_{BM}(\chi)/U_A$ for BC), as shown in Figure S6(A), in that the anti-symmetric normalized velocity and pressure profiles ($V_{BM}(\chi)/U_A$, $\Delta V_{BM}(\chi)/U_A$, and $P_A(\chi)/U_A$) all feature overlapping lines for their different excitation cases.

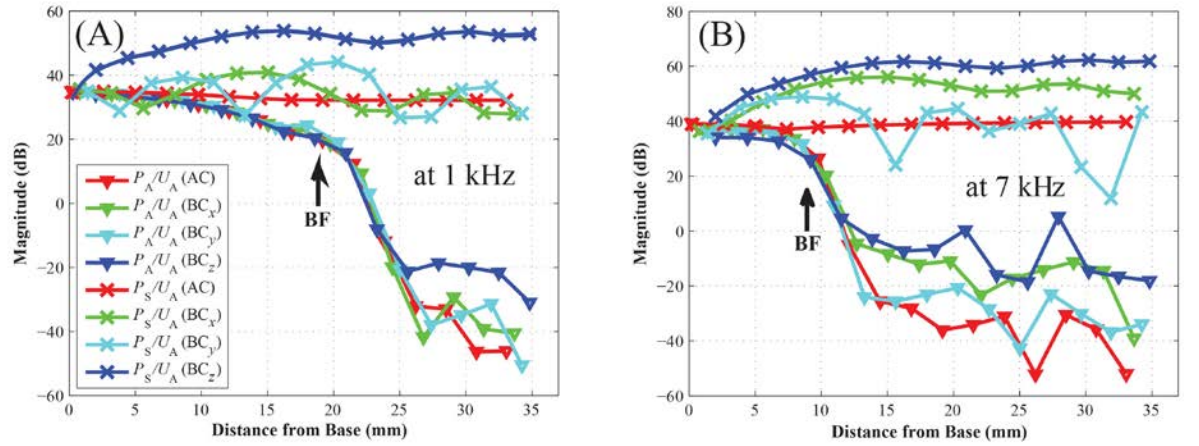

FIGURE S7. (A and B) Cochlear scalae-fluid pressure distributions along the BM length (*i.e.*, the anti-symmetric pressure, $P_A(\chi)$, and symmetric pressure, $P_S(\chi)$), in response to AC and BC excitations, normalized by the corresponding anti-symmetric volume-velocity component, U_A, at (A) 1 kHz and (B) 7 kHz.

Comparisons with the simplified box model

Based on a simplified box cochlear model, the BM was shown to primarily respond to the anti-symmetric excitation components (*i.e.*, the slow traveling wave; 10) generated at the OW and RW, regardless of whether the components were produced via AC or BC excitation (1). In this study, the relationships between the anti-symmetric pressure and volume-velocity components were investigated using a more anatomically realistic coiled cochlear model. As shown in Figure S6, regardless of the excitation type, the BM-velocity response was correlated with the anti-symmetric rather than the symmetric volume velocity. In addition, Figure S7 shows that the anti-symmetric volume velocity was closely related to the anti-symmetric pressure along the BM length. In short, regardless of the excitation type or direction, the anti-symmetric scalae-fluid pressure and anti-symmetric volume velocity are both highly correlated with the BM velocity. These results from the coiled model are consistent with those from the simplified box model.

SUPPORTING MATERIAL REFERENCES

1. Kim, N., K. Homma, and S. Puria. 2011. Inertial bone conduction: Symmetric and anti-symmetric components. *J. ARO.* 12:261-279.
2. Gan, R.Z., B.P. Reeves, and X. Wang. 2007. Modeling of Sound Transmission from Ear Canal to Cochlea. *Ann. Biomed. Eng.* 32: 847-859.
3. Puria, S., W.T. Peake, and J.J. Rosowski. 1997. Sound-pressure measurements in the cochlea vestibule of human cadaver ears. *J. Acoust. Soc. Am.* 101:2754-2770.
4. Aibara, R., J.T. Welsh, S. Puria, and R.L. Goode. 2001. Human middle-ear sound transfer function and cochlear input impedance. *Hear. Res.* 152:100-109.
5. Nakajima, H.H., W. Dong, E.S. Olson, S.N. Merchant, M.E. Ravicz, and J.J. Rosowski. 2009. Differential intracochlear sound pressure measurements in normal human temporal bones. *J. ARO.* 10:23-36.
6. Merchant, S.N., M.E. Ravicz, and J.J. Rosowski. 1996. Acoustic input impedance of the stapes and cochlea in human temporal bones. *Hear. Res.* 97:30-45.
7. Gundersen, T., Φ. Skarstein, and T. Sikkeland. 1978. A study of the vibration of the basilar membrane in human temporal bone preparations by the use of the Mössbauer effect. *Acta Otolaryngol.* 86:225-232.
8. Stenfelt, S., S. Puria, N. Hato, and R.L. Goode. 2003. Basilar membrane and osseous spiral lamina motion in human cadavers with air and bone conduction stimuli. *Hear. Res.* 181:131-143.
9. Greenwood, D.D. 1990. A cochlear frequency-position function for several species-29 years later. *J. Acoust. Soc. Am.* 87:2592-2605.
10. Peterson, L.P., and B.P. Bogart. 1950. A dynamical theory of the cochlea. *J. Acoust. Soc. Am.* 22:369-380.